Unusual Kinetic Behavior of the Reactions Mg + O_2 + M and Ca + O_2 + M (M = N_2, He) over Extended Temperature Ranges

Chia-Fu Nien and B. Rajasekhar†

Rosenstiel School of Marine and Atmospheric Science, University of Miami, 4600 Rickenbacker Causway, Miami, Florida 33149

John M. C. Plane*

School of Environmental Sciences, University of East Anglia, Norwich, NR4 7TJ, United Kingdom

Received: January 28, 1993; In Final Form: March 22, 1993

The reaction Mg + O_2 + N_2 was studied by a static-flow technique in which the rate coefficient was determined relative to the diffusion coefficient of Mg(^{1}S) atoms in N_2. This yielded $k(349\text{K}<T<625\text{K}) = (2.15 \pm 0.56) \times 10^{-30} \exp[-(19.5 \pm 0.7)\ \text{kJ mol}^{-1}/RT]$, where the quoted uncertainty is 2σ. This result is in very good accord with the results of a recent flow-tube study which found the rate coefficient to be about 3 times slower when He was the third body. The reaction Ca + O_2 + M (M = N_2, He) was then studied by the pulsed laser photolysis of a Ca atom precursor, followed by time-resolved laser-induced fluorescence of the resulting Ca(^{1}S) atoms. The reaction with N_2 as the third body is between 2 and 3 times faster than the reaction with He, and the rate coefficients for both third bodies increase between 218 and 340 K and then decrease up to 1100 K. *Ab initio* calculations and RRKM theory are then employed to demonstrate that the unusual temperature dependences of both the Mg and Ca reactions are most probably caused by barriers in the entrance channels of these reactions. The recommended rate coefficients between 120 and 2000 K are then given by $\log_{10}(k(\text{Mg+O}_2\text{+N}_2)) = -392.7 + 439.1x - 203.2x^2 + 42.56x^3 - 3.413x^4$, $\log_{10}(k(\text{Mg+O}_2\text{+He})) = -394.5 + 442.4x - 205.0x^2 + 42.94x^3 - 3.436x^4$, $\log_{10}(k(\text{Ca+O}_2\text{+N}_2)) = -97.75 + 84.66x - 39.85x^2 + 8.522x^3 - 0.7093x^4$, and $\log_{10}(k(\text{Ca+O}_2\text{+He})) = -93.67 + 78.02x - 35.76x^2 + 7.369x^3 - 0.5899x^4$, where k is in units of cm^6 molecule^{-2} s^{-1}, $x = \log_{10}(T)$, and the uncertainty in k is estimated to be ±30%. Finally, the implications of these results for the chemistry of meteor-ablated Mg and Ca in the upper atmosphere are considered.

Introduction

The reactions

$$\text{Mg}(^1\text{S}) + \text{O}_2 + \text{M} \rightarrow \text{MgO}_2 + \text{M} \quad (\text{M = third body}) \quad (1)$$

$$\text{Ca}(^1\text{S}) + \text{O}_2 + \text{M} \rightarrow \text{CaO}_2 + \text{M} \quad (2)$$

are unusual examples of metal + O_2 recombination reactions because the Group 2 metal atoms are *closed*-shell species. Thus, these reactions are not radical–radical processes like the analogous reactions of the Group 1 metal atoms.[1,2] Nevertheless, both MgO_2 and CaO_2 are known from matrix-isolation studies[3,4] to be superoxides, existing predominantly as ion pairs, e.g., $Ca^+(O_2)^-$. This ionic character has also been confirmed by *ab initio* quantum studies.[1,2,5] Reactions 1 and 2 thus involve a crossing from a long-range covalent attractive surface onto a close-range ionic potential surface, at metal atom–O_2 separations of approximately 2.0 and 2.5 Å, respectively.[6] This type of covalent/ionic curve crossing, accompanied by the relatively high densities of vibrational states which characterize ionic molecules, has been shown to enhance dramatically the rates of recombination between Group 1 metal atoms and species such as OH,[7] I,[8] and O_2.[1,9]

An important motivation for studying reactions 1 and 2 is to initiate a study of the chemistry of the Group 2 metal atoms which ablate from meteoroids in the earth's upper atmosphere.[10] Mg is one of the most abundant metals in meteoritic minerals, making up about 50% (by weight) of the total input of metals from extraterrestrial sources into the atmosphere. Lidar (laser radar) observations have established that several of the meteoric metals, namely, Na, K, Li, Ca, and Fe, exist as thin layers of neutral metal atoms at about 90-km altitude. However, atomic Mg cannot be observed in the mesosphere by ground-based lidar or photometry because the Mg(3^1P–3^1S) resonance line at 285.21 nm is obscured by the Hartley band of ozone in the lower atmosphere.[10] Thus, in the absence of any rocket- or satellite-based observations of atomic Mg, knowledge of the atmospheric chemistry of this metal has to be obtained from laboratory measurements, coupled with atmospheric models.[10]

In the case of Ca, the summertime column abundance of the atomic Ca layer at 90 km is depleted by a factor of about 120 relative to that of the Na layer,[11] even though Ca and Na have similar abundances in most meteoritic minerals.[10] This depletion increases by a factor of about 3 in winter.[11] The reason for this relative absence of atomic Ca remains to be established. However, by analogy with the atmospheric chemistry of Na,[10] CaO_2 and MgO_2 could be important sinks for these Group 2 metals in the mesosphere, particularly if reactions 1 and 2 are as fast as the analogous reaction of Na.[1]

Reaction 1 has been studied previously by Vinckier *et al.*,[2] who employed the fast flow-tube technique with He as the carrier gas. They found that reaction 1 was very slow, with a *positive* temperature dependence. Hodgson and Mackie[12] carried out a shock-tube study of the *bimolecular* reaction

$$\text{Mg} + \text{O}_2 \rightarrow \text{MgO} + \text{O} \quad (3)$$

and obtained $k_3(2000\text{K}) = (8 \pm 5) \times 10^{-14}$ cm^3 molecule^{-1} s^{-1}. Kashireninov *et al.*[13] studied reaction 3 in a diffusion flame, which yielded $k_3(873\text{–}1023\text{K}) = (4.8 \pm 0.5) \times 10^{-10} \exp[(-71.1 \pm 7.9\ \text{kJ mol}^{-1})/RT)]$ cm^3 molecule^{-1} s^{-1}. These studies are in very poor agreement. Moreover, reaction 3 is endothermic by 134–237 kJ mol^{-1}, the uncertainty arising from the spread of estimates for D_0(Mg–O) values which range from a recent high-level *ab*

* To whom correspondence should be addressed.
† Present address: Brookhaven National Laboratory, Upton, Long Island, NY 11973.

0022-3654/93/2097-6449$04.00/0

initio calculation[14] of 265 kJ mol^{-1} to the older value of 334 ± 25 kJ mol^{-1} recommended by the JANAF tables.[15] However, the activation energy obtained in the diffusion flame study[13] is outside this range, so this study appears to be in error; furthermore, the shock-tube study[12] is only in accord with the upper limit of the older value of D_0(Mg–O).[14]

Reaction 2 does not appear to have been studied previously. However, Kashireninov *et al.*[13] investigated the reaction

$$Ca + O_2 \rightarrow CaO + O \quad (4)$$

by the diffusion flame technique and found k_4(1040–1200K) = $(3.5 \pm 0.3) \times 10^{-10} \exp[(-61.9 \pm 8.4 \text{ kJ mol}^{-1})/RT]$ cm^3 molecule^{-1} s^{-1}. The activation energy appears to be in better agreement, although it is still smaller than the reaction endothermicity, which is 96 kJ mol^{-1} if the most recent *ab initio*[14] and experimental[16] value for D_0(Ca–O) of *ca.* 397 kJ mol^{-1} is adopted.

In this paper, we will report the measurement of $k_1(T)$ by a new static-flow system which we developed recently to study the reaction Mg + N_2O[17] and the measurement of $k_2(T)$ by a two-laser pulse/probe technique.[18] The bond energies of MgO_2 and CaO_2, and the nature of the entrance channel of the potential energy surface for Mg + O_2, will then be determined through *ab initio* quantum calculations. These theoretical results will be coupled with simplified Rice–Ramsberger–Kassel–Marcus (RRKM) theory[19] in order to interpret the experimental results and then to extrapolate $k_1(T)$ and $k_2(T)$ to temperatures outside the experimentally accessible range. Finally, we will discuss the significance of reactions 1 and 2 with respect to the chemistry of Mg and Ca in the upper atmosphere.

Experimental Section

Mg + O_2 + N_2. Reaction 1 was studied over the temperature range 350–624 K by the static-flow technique, which we designed to study the gas-phase reaction of a refractory species that is relatively slow, so that diffusional loss to the walls of the reactor can be made comparable to chemical loss in the gas phase.[17] Thus, k_1 was determined relative to the diffusion coefficient of Mg in N_2. This new technique has been described in detail recently,[17] so only a brief description is given here. The stainless steel reactor, which is illustrated in ref 10, consists of a central cylindrical chamber where the reaction was studied. This chamber is enclosed in a furnace which permits the chamber temperature to be varied from 300 to 1100 K. Alternatively, the furnace can be filled with powdered solid CO_2 to cool the chamber to below 250 K. The chamber is also at the intersection of four horizontal side arms which are mutually orthogonal. In this study, one pair of opposite (i.e., collinear) side arms provided the optical coupling for a Mg hollow-cathode lamp, which was focused into the center of the chamber, as well as the means by which flows of O_2, diluted in N_2, entered the chamber. The third side arm was independently heated to act as a source of Mg atoms, produced by heating Mg metal chips to 600–700 K and entraining the resulting Mg vapor in a flow of N_2 into the central chamber. The fourth side arm served as an exit for the gas flows to the pump. A fifth vertical side arm provided the coupling for the photomultiplier tube (Thorn EMI Gencom Inc., Model 9816QB), which monitored the fluorescence signal at 285.21 nm (Mg(3^1P–3^1S)) after passing through an interference filter centered at 285 nm (Microcoatings, Model ML3-285, fwhm = 10 nm). A fast photon-counting system (Thorn EMI Model Aped-II amplifier–discriminator and EG&G Ortec ACE-MCS multichannel scaler) was then employed to detect the fluorescence signal, with care being taken to ensure that the fluorescence signal was linearly proportional to the Mg concentration in the chamber.[17]

The steady-state concentration of Mg in the chamber was a balance between input from the heat pipe, reaction with O_2 in the gas phase, and deposition onto the walls of the chamber. For an experimental run, the input of Mg vapor and the rate of deposition were kept constant by fixing the flow conditions, i.e., pressure, total flow, and turnover (residence) time in the chamber. The steady-state Mg atom concentration in the center of the chamber was then measured as a function of excess O_2 concentration, relative to the Mg concentration in the absence of O_2. Hence, k_1 was determined relative to the diffusion of Mg to the chamber walls.[17]

Ca + O_2 + M. Reaction 2 was investigated by the technique of time-resolved laser-induced fluorescence spectroscopy of Ca atoms following the pulsed photolysis of a Ca atom precursor in an excess of O_2 and the bath gas (N_2 or He). The same reactor was employed, but now one pair of opposite horizontal side arms provided the optical coupling for the pulse and probe lasers into the central chamber where the reaction was initiated. Either Ca acetyl acetonate (Ca[$C_5H_7O_2$]$_2$), hereafter referred to as CaAcAc, or CaI_2 was employed as the Ca atom precursor. Powdered samples of these salts were placed in a tantalum boat in the heat pipe and then heated to about 420 K in the case of CaAcAc or about 940 K for CaI_2 (the concentration of the CaI_2 vapor in equilibrium above the molten salt was then 2.9×10^{12} molecules cm^{-3} [15]). The salt vapor was entrained in a flow of the bath gas and carried into the central chamber. When the central chamber was at a lower temperature than the heat pipe, there was a major loss of the salt vapor through deposition onto the relatively cool chamber walls. Nevertheless, sufficient vapor reached the center of the chamber to be photolyzed using an ArF excimer laser (Questek, Model 2110, energy 20–50 mJ pulse^{-1}). The excimer beam was shaped by a system of lenses and a pinhole and then focused into the middle of the central chamber.

The resulting Ca(^{1}S) atoms were probed at 422.7 nm (Ca(4^1P$_1$–4^1S)) using a nitrogen-pumped dye laser (Laser Science Inc., Model VSL-337; laser dye Stilbene 420, bandwidth = ca. 0.01 nm). In these experiments, the excimer and dye lasers were arranged to be collinear and counterpropagating, with the dye laser protected from the excimer beam by a dichroic filter (Newport Corp., Model 10QM20HL1, wavelength cut-on at 400 nm). The diameter of the dye laser was maintained to be about 80% that of the excimer, by means of a beam expander. Resonant LIF was recorded using a gated integrator (Stanford Research Systems, Model SR250) interfaced to a microcomputer, after passing through an interference filter centered at 420 nm (Oriel Corporation, fwhm = 10 nm).

Materials. Nitrogen, 99.9995% purity (Liquid Carbonic) and Helium, 99.9999% (Matheson "Matheson Purity") were used without further purification. O_2, 99.995% pure (Liquid Carbonic), was trapped at 77 K and pumped on before use. The metallic samples were heated in the heat pipe for about 1 h prior to kinetic experiments in order to remove volatile impurities: Mg metal chips, 99.95+% (Aldrich) at 600 K; CaI_2 99%+ (Aldrich, Anhydrous) at 700–850 K; and CaAcAc (Chem Service) at 370 K.

Results

Mg + O_2 + N_2. In the static-flow experiment, the steady-state concentration of Mg vapor in the central chamber, $[Mg]_{ss}$, is given by

$$d[Mg]/dt = F - k_1[O_2][N_2][Mg]_{ss} - k_{diff}[Mg]_{ss} = 0 \quad (5)$$

where F is the rate of input of Mg vapor from the heat pipe and k_{diff} is the rate of diffusional loss of Mg vapor by deposition onto the walls of the chamber. Use of eq 5 assumes that the loss of Mg vapor by flowing into the exit side arm of the reactor is much smaller than loss by either chemical reaction or deposition on the walls and that the Mg vapor is well-mixed in the central chamber. Both of these conditions were met by ensuring that the turnover time in the central chamber was at least a factor of 20 longer than $1/k_{diff}$.

We have shown previously[17] how k_{diff} may be determined from the solution of the diffusion equation for cylindrical geometry.[20]

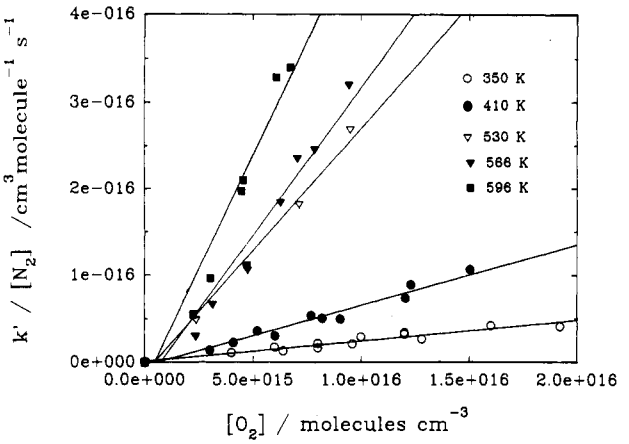

Figure 1. Plots of $k'/[N_2]$ vs $[O_2]$, where $k' = k_{diff}(([Mg]_o/[Mg]_{ss}) - 1)$, from the study of Mg + O_2 + N_2 over a range of temperatures. The $[N_2]$ range was (2.0–8.2) × 10^{17} cm^{-3}. The solid lines are linear regression curves through the data at each temperature.

TABLE I: Experimental Determination of k(Mg+O_2+N_2) as a Function of T (Quoted Uncertainty Is 2σ)

T/K	P/Torr	D(Mg–N_2)[a]/ (Torr cm^2 s^{-1})	$k/10^{-33}$ cm^6 $molecule^{-2}$ s^{-1}
350	15.0	354 ± 17	2.88 ± 0.29
350	24.0	354 ± 17	2.16 ± 0.20
350	30.0	354 ± 17	2.71 ± 0.62
410	20.0	393 ± 44	8.36 ± 2.45
410	25.0	393 ± 44	7.01 ± 0.81
419	15.0	406 ± 49	6.95 ± 1.90
530	11.7	572 ± 117	28.3 ± 9.6
566	15.0	628 ± 143	35.8 ± 16.1
566	20.0	628 ± 143	31.5 ± 13.6
577	24.2	645 ± 152	35.1 ± 26.8
596	15.0	676 ± 167	51.9 ± 26.4
624	12.7	721 ± 190	34.8 ± 18.4

[a] k_{diff} is then equal to $0.800D(Mg–N_2)/P$, where P is the reactor pressure in Torr.

This procedure also requires an estimate of the binary diffusion coefficient for Mg atoms in N_2, D(Mg–N_2). We have previously derived this quantity relative to D(Na–N_2),[17] which is known independently from experiment.[9a,21,22]

If $[Mg]_o$ is the steady-state Mg concentration in the absence of O_2, i.e., when the input flow from the heat pipe is balanced only by deposition onto the chamber walls, and if the total flow and pressure are kept constant while the O_2 concentration is varied, it follows from eq 5 that

$$[Mg]_o/[Mg]_{ss} = k_1[O_2][N_2]/k_{diff} + 1 \qquad (6)$$

Hence, a plot of $k_{diff}([Mg]_o/[Mg]_{ss} - 1)/[N_2]$ versus $[O_2]$ should be linear, passing through the origin with a slope of k_1. Such plots are illustrated in Figure 1. The linear regression lines, fitted to the data at each temperature, all pass through the origin within their 2σ uncertainties. The resulting values of k_1 are listed in Table I, along with the pressures in the central chamber at which each k_1 was measured. The values of D(Mg–N_2), calculated at each experimental temperature, are also given in Table I. The quoted uncertainties of k_1 include both the 2σ uncertainties from the linear regression fits to the plots of $k_{diff}([Mg]_o/[Mg]_{ss} - 1)/[N_2]$ versus $[O_2]$ and the uncertainties in k_{diff}. At several temperatures, k_1 was determined as a function of pressure (see Table I). Figure 2 illustrates plots of $k_{diff}([Mg]_o/[Mg]_{ss} - 1)$ versus $[O_2]$ for three different pressures of N_2 at 350 K. This indicates that the loss of Mg is proportional to $[N_2]$, within the experimental uncertainty, thereby confirming that reaction 1 is indeed termolecular.

The lower temperature limit in this experiment resulted from reaction 1 being too slow, relative to diffusion, below 350 K. In principle, this limitation could have been overcome by increasing the concentrations of O_2 and N_2, which would have increased the rate of reaction 1 and decreased k_{diff}. In practice, however, an increase in the total pressure in the reactor caused too large a fraction of the Mg vapor flow to be lost through deposition on the cool walls of the heat pipe at the entrance to the cold central chamber. Also, if the O_2 concentration were increased substantially relative to that of N_2, then O_2 would have become a significant third body, and diffusion of Mg atoms through O_2 could no longer have been ignored.[17] The upper temperature limit was caused by the background-scattered light signal, arising from black-body radiation from the hot reactor surfaces, becoming substantially larger than the atomic Mg resonance fluorescence signal, even though the interference filter has a transmission/blocking factor of about 3000:1.

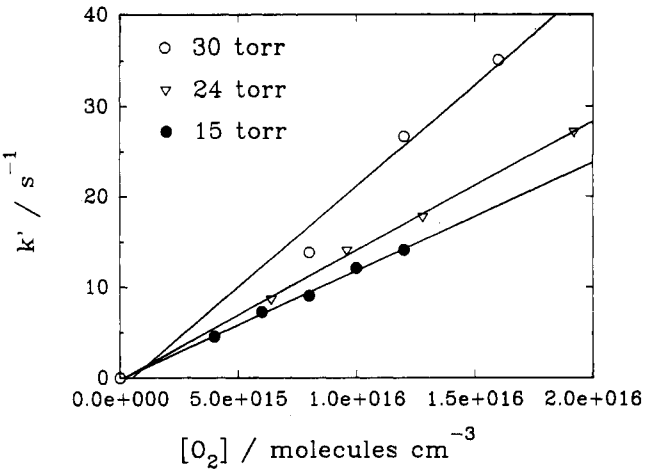

Figure 2. Plots of k' vs $[O_2]$, where $k' = k_{diff}(([Mg]_o/[Mg]_{ss}) - 1)$, from the study of Mg + O_2 + N_2 at 350 K. The solid lines are linear regression curves through the data for three different pressures of N_2.

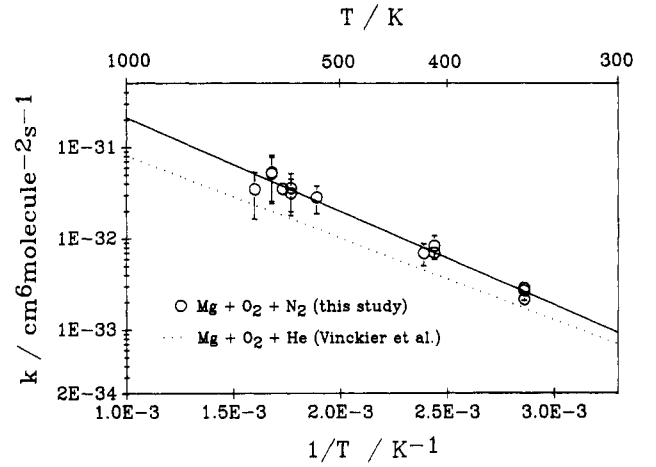

Figure 3. Arrhenius plots ($\ln(k_1)$ against $1/T$) for the reaction Mg + O_2 + M (M = N_2 or He) over the temperature range 300–1000 K, comparing the results from this study with those of Vinckier *et al.* (ref 2).

Figure 3 is an Arrhenius plot of reaction 1, illustrating the data in Table I. A weighted fit of the data to the simple Arrhenius form yields (at the 2σ level of uncertainty)

$$k_1(350K<T<624K) = (2.15 \pm 0.56) \times 10^{-30} \times \exp[-(19.5 \pm 0.7 \text{ kJ mol}^{-1})/RT] \text{ cm}^6 \text{ molecule}^{-2} \text{ s}^{-1} \qquad (7)$$

It should be noted that this result is marginally different from the result of a preliminary report of this study.[1] Finally, the data for reaction 1 are plotted in Figure 4 in the conventional manner for a recombination reaction, i.e., $\ln(k_1(T))$ vs $\ln(T)$.

Ca + O_2 + M. We have demonstrated previously[18] that the photolysis of CaI_2 at 193 nm, to yield Ca atoms, is a multiphoton

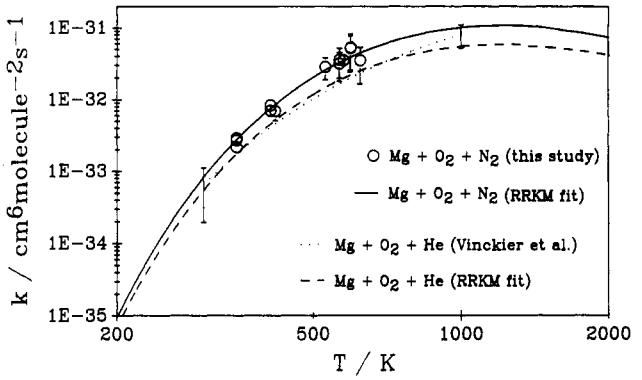

Figure 4. Plots of k_1 vs T for the reaction Mg + O_2 + M (M = N_2 or He), comparing experimental results from the present study and from Vinckier *et al.* (ref 2), with extrapolations of $k_1(T)$ over the temperature range 200–2000 K obtained by using the Troe formalism (ref 19).

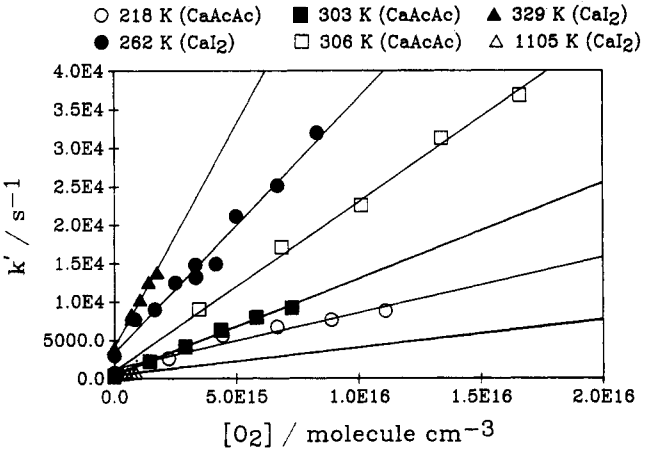

Figure 5. Plots of k' vs $[O_2]$ for the reaction Ca + O_2 + N_2 as a function of temperature, pressure, and Ca atom precursor. The concentrations of N_2 were as follows: 6.17×10^{17} molecule cm^{-3} (218 K), 2.21×10^{18} molecule cm^{-3} (262 K), 3.80×10^{17} molecule cm^{-3} (303 K), 8.82×10^{17} molecule cm^{-3} (306 K), 1.88×10^{18} molecule cm^{-3} (329 K), and 3.15×10^{17} molecule cm^{-3} (1105 K). The solid lines are linear regressions curves through the data.

process. This was also found to be the case in the present study when employing CaAcAc as the precursor: the yield of Ca atoms was found to depend approximately quadratically on the excimer laser pulse energy. Since the concentrations of O_2 and the bath gas were always well in excess of the concentration of Ca atoms resulting from the pulsed photolysis of CaI_2 or CaAcAc vapor, the loss of Ca atoms should be described by the pseudo-first-order decay coefficient, k', where

$$k' = k_{difn} + k_2[O_2][M], \quad M = N_2 \text{ or He} \qquad (8)$$

The term k_{difn} describes diffusion of the Ca atoms out of the volume defined by the laser beams and within the field of view of the PMT.[23] Over the temperature range studied, the observed decays of the LIF signal were of a simple exponential form, $A \exp(-k't)$.

When the dependence of k' on $[O_2]$ was studied, the bath gas pressure was kept constant so that k_{difn} appeared as an intercept on a plot of k' vs $[O_2]$. Plots of k' vs $[O_2]$ are illustrated in Figure 5 for a selection of the temperatures at which reaction 1 was studied. k' exhibits a clear linear dependence on $[O_2]$. Inspection of Figure 5 indicates that k_{difn} varied from about 500 to 3000 s^{-1}. This range of values mostly resulted from having to vary the waist height of the focused excimer laser beam in the central chamber, in order to obtain the necessary yield of Ca atoms. For instance, tight focusing was particularly required for photolyzing CaI_2 at low temperatures.

The slopes of the plots of k' vs $[O_2]$ thus yield $k_2[M]$ ($=k''$) as a function of temperature. Figures 6 and 7 illustrate plots of

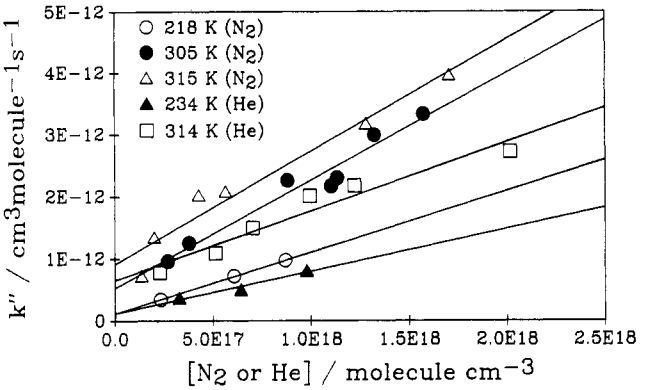

Figure 6. Plots of k'' vs [M], where k'' is defined in the text, for the study of Ca + O_2 + M (M = N_2 or He), as a function of temperature and third body. The Ca atom precursor is CaAcAc. The solid lines are linear regression curves through the data.

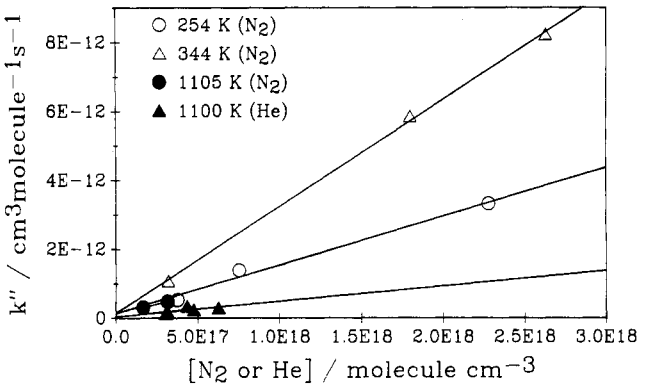

Figure 7. Plots of k'' vs [M], where k'' is defined in the text, for the study of Ca + O_2 + M (M = N_2 or He), as a function of temperature and third body. The Ca atom precursor is CaI_2. The solid lines are linear regressions curves through the data.

k'' vs [M] for the Ca atom precursors CaAcAc and CaI_2, respectively. These plots confirm the termolecular nature of reaction 2. The plots in Figure 7 pass through the origin within their experimental uncertainties, as expected from eq 8. However, the plots in Figure 6 have positive intercepts which increase with temperature. We believe that the cause of this was a slow gas-phase reaction between CaAcAc and O_2, once they mixed in the central chamber. One of the reaction products, probably an alkyl peroxy radical, then reacted relatively rapidly with the Ca(^{1}S) formed in the photolysis pulse. In order for this side reaction to appear as an intercept in a plot of k'' vs [M], this product must have been produced in quantities proportional to the O_2 concentration in the chamber. This is supported by the observation that the intercepts of these plots were about the same for both the third bodies studied, whereas the slopes, which yield k_2, are significantly steeper for N_2 than for He (Figure 6).

Table II contains a list of k_2 (M = N_2, He) as a function of T. These data are illustrated in Figure 8, which reveals satisfactory agreement between the results obtained with CaI_2 and CaAcAc. The lower temperature limit of 216 K in these experiments was prescribed by the choice of the refrigerant and the requirement to maintain the heat pipe at the required elevated temperatures (see above). The upper temperature of about 1100 K is limited by the stainless steel from which the reactor is constructed. We also found that kinetic measurements could not be carried out satisfactorily between about 400 and 1000 K. This was because the decomposition of CaAcAc, even in the absence of O_2, became very rapid compared with the turnover time of the gas mixture in the central chamber. In the case of CaI_2, O_2 appeared to react with this salt on the hot reactor walls to release I_2, which is very reactive toward many metal atoms with low ionization energies.[6,24] Indeed, we observed a significant kinetic

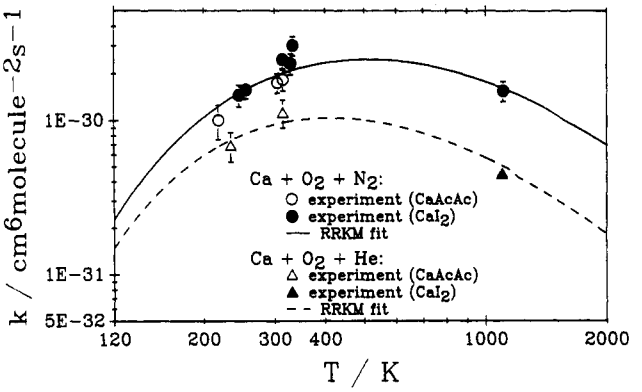

Figure 8. Plots of k_2 vs T for the reaction Ca + O_2 + M (M = N_2 or He), comparing the experimental results from the present study with extrapolations of $k_2(T)$ over the temperature range 120–2000 K obtained by using the Troe formalism (ref 19).

TABLE II: Experimental Determination of k_2(Ca+O_2+M) as a Function of T (Quoted Uncertainty Is 2σ)

T/K	P/Torr	$k_1/10^{-30}$ cm^6 molecule^{-2} s^{-1}	precursor
		Ca + O_2 + N_2	
216–219	5.3–19.8	0.93 ± 0.30	CaAcAc
245	40.5	1.21 ± 0.36	CaI_2
250–262	10.0–60.5	1.35 ± 0.32	CaI_2
300–310	8.6–50.0	1.74 ± 0.25	CaAcAc
310–317	25.7–39.6	2.44 ± 0.31	CaI_2
311–320	4.5–55.0	1.82 ± 0.28	CaAcAc
329–335	11.5–94.4	3.00 ± 0.43	CaI_2
1107	19.2–36.3	1.54 ± 0.38	CaI_2
		Ca + O_2 + He	
232–234	8.0–23.9	0.68 ± 0.27	CaAcAc
311–318	7.5–65.9	1.12 ± 0.28	CaAcAc
1100	35.0–72.0	0.45 ± 0.10	CaI_2

interference above 400 K, presumably from the reaction Ca + I_2 → CaI + I. We have observed the same problem with the Group 1 metal iodide precursors.[9b] However, above 1000 K, the equilibrium between I_2 and I is well over to the atomic side,[15] so this interference disappears.[9b]

Discussion

Mg + O_2 + M. Vinckier *et al.*[2] measured k_1(M=He) = (6.4 ± 1.5) × 10^{-31} exp([(17.2 ± 0.8) kJ mol^{-1}/RT] cm^6 molecule^{-2} s^{-1} in their fast flow-tube study. This result is illustrated in Figures 3 and 4. Comparison with the present measurement of k_1(M=N_2), i.e., eq 7, demonstrates excellent agreement. The temperature dependences of both third bodies are very similar, with N_2 being about 3 times more efficient than He. Over the temperature ranges of the present study and that of Vinckier *et al.*,[2] the bimolecular reaction 3 is so endothermic (see Introduction) that k_3 must be too small, by a factor of at least 10^4, to compete with the recombination reaction 1.

Two striking differences between reaction 1 and the analogous reactions of metal atoms in other periodic groups[1,2] are the positive temperature dependence of k_1 and that k_1 is smaller by about 3 orders of magnitude. Both of these differences are evidence of a substantial barrier on the potential energy surface (PES) of reaction 1. Indeed, Andrews *et al.*[4] found that Mg and O_2 did not react together in their matrix-isolation experiments and instead produced MgO_2 from the reaction Mg + O_3.

We therefore explored the nature of this barrier by means of *ab initio* calculations, which were carried out using the Gaussian 86 suite of programs.[25] Following our previous work on LiO_2 and NaO_2,[26] we employed the 6-31G* basis set, which is a large flexible basis set including d functions on the atoms. This basis set appears to be adequate for the analysis which follows. In reaction 1, Mg(^{1}S) and $O_2(^3\Sigma_g^-)$ correlate with triplet MgO_2 by an adiabatic curve crossing onto the triplet ionic diabat arising from $Mg^+(^2S)$ and $O_2^-(^2\Pi)$. It should be noted that these ionic species also correlate with singlet MgO_2, and nonadiabatic transitions with respect to spin are known to occur in reactions of Mg(^{1}S) atoms.[17] However, since the probability of such transitions is usually small,[17] and Bauschlicher *et al.*[5] have shown recently that $MgO_2(^1A_1)$ is only slightly bound with respect to Mg and O_2, we have ignored the role of the singlet ground-state surface of MgO_2. Three triplet geometries were examined: linear Mg–O–O, linear O–Mg–O, and the isosceles triangular (C_{2v}) form. These geometries were optimized at the Hartree–Fock single-configuration level, and the bond energies were then computed from the relation

$$D_e(\text{Mg–O}_2) = E(\text{Mg}^+) + E(\text{O}_2^-) - E(\text{MgO}_2) - \text{IP(Mg)} + \text{EA(O}_2) \quad (9)$$

where E indicates the absolute electronic energy; IP(Mg) is the ionization potential of Mg and EA(O_2) is the electron affinity of oxygen, both of which are known accurately from experiment.[15] The advantage of this method of calculating the bond energy of an ionic molecule (by isogyric dissociation) has been discussed elsewhere.[5,26]

The results of these calculations are shown in Table III, where comparison is made with other theoretical work.[2,5] The MgO_2-($^3A_2$) state with C_{2v} geometry is adequately described by a single configuration,[5] and the differences in the geometry and bond energy are largely related to the choice of basis set. For example, if diffuse functions are included in the basis set, then a calculation at the HF/6-31++G(d,p) level yields D_e(Mg–O_2) = 62 kJ mol^{-1}, which is very close to the result of Vinckier *et al.*[2] By contrast, the linear geometries of MgO_2 give rise to numbers of near-

TABLE III: Comparison of *ab Initio* Geometries and Bond Energies for MgO_2

	state	r_{Mg-O}/Å	r_{O-O}/Å	D_e(Mg–O_2)/ (kJ mol^{-1})
		O–Mg–O, C_{2v} Geometry		
this study (HF/6-31G*)	$^3A_2$	1.98	1.30	129
Bauschlicher *et al.*[5]	$^3A_2$	1.97	1.36	95
Vinckier *et al.*[2]	$^3A_2$	1.97	1.38	62
		Linear O–Mg–O		
this study (HF/6-31G*)	$^3\Sigma_u^-$	1.77	–	109
Bauschlicher *et al.*[5]	$^3\Sigma_g^-$	1.85	–	106
		Linear Mg–O–O		
this study (HF/6-31G*)	*a*	1.80	1.30	77

[a] Electronic symmetry not determined.

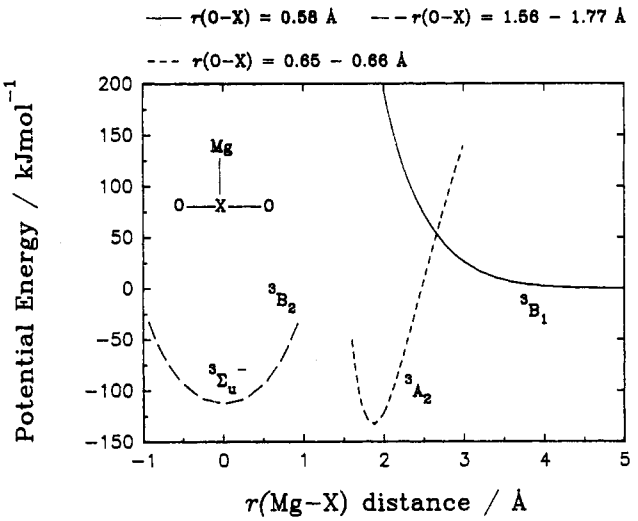

Figure 9. Potential energy surfaces for the reaction Mg + O_2 along the C_{2v} axis. The surfaces were calculated at the HF/6-31G* level as a function of r(Mg–X) by constraining the r(O–X) distance as indicated.

TABLE IV: Extrapolation of Rate Data for the Reaction Mg + O_2 + M[a]

Input Parameters for the $MgO_2(^3\Sigma_g^-)$ Molecule

r_{Mg-O} = 1.85 Å, I = 109.5 amu Å^2, ν_1 = 533 cm^{-1}, ν_2 = 152 cm^{-1} (×2), ν_3 = 796 cm^{-1}, D_0(Mg–O_2) = 106 kJ mol^{-1}, E_b = 26 kJ mol^{-1}, E_0 = 132 kJ mol^{-1}

Data for Mg + O_2 + N_2 at 350 K

$\sigma(MgO_2–N_2)$ = 5.0 Å, $\epsilon(MgO_2–N_2)/k$ = 500 K, Z_{LJ} = 9.04 × 10^{-10} cm^3 molecule^{-1} s^{-1}, s = 4, m = 3, r = 0, Q_{vib} = 5.42, a = 0.987, $\rho(E_0)$ = 2.36, F_E = 1.06, F_{anh} = 1.73, F_{rot} = 17.3, F_{corr} = 1, K_{eq} = 5.41 × 10^{-9} cm^3 molecule^{-1}, k_0^{sc} = 7.24 × 10^{-25} cm^3 molecule^{-1} s^{-1}, $k_{rec,0}^{sc}$ = 3.91 × 10^{-33} cm^6 molecule^{-2} s^{-1}, β_c = 0.70, $\langle\Delta E\rangle$ = –13.4$(T/350)^{-0.4}$ kJ mol^{-1}

Data for Mg + O_2 + He at 350 K

$\sigma(MgO_2–He)$ = 4.5 Å, $\epsilon(MgO_2–He)/k$ = 450 K, Z_{LJ} = 1.56 × 10^{-9} cm^3 molecule^{-1} s^{-1}, k_0^{sc} = 1.25 × 10^{-24} cm^3 molecule^{-1} s^{-1}, $k_{rec,0}^{sc}$ = 6.72 × 10^{-33} cm^6 molecule^{-2} s^{-1}, β_c = 0.25, $\langle\Delta E\rangle$ = –1.63$(T/350)^{0.0}$ kJ mol^{-1}

[a] For the definition of symbols not in the present text, see ref 19.

degenerate states, which are not well-represented by a single configuration.[5] The results from the present study should therefore not be considered to be very reliable and are included here primarily for illustrative purposes (see below). Linear Mg–O–O appears to be much less stable than $MgO_2(^3A_2$ or $^3\Sigma_u^-)$. Bauschlicher *et al.*[5] have recently performed a high-level calculation on linear O–Mg–O and found that the lowest-lying linear state is actually $MgO_2(^3\Sigma_g^-)$. This is, in fact, more stable than $MgO_2(^3A_2)$ by about 11 kJ mol^{-1}.[5]

In order to investigate the dynamics of reaction 1, we now consider some of the relevant potential energy surfaces, starting with the special case of reaction along the C_{2v} axis, as shown in Figure 9. The potential energy curves in Figure 9 were calculated at the HF/6-31G* level and are plotted as a function of r(Mg–X), which is defined in the figure. The $^3B_1$ and $^3A_2$ curves were obtained by fixing r(O–O) at 1.16 and 1.30 Å, corresponding to the O–O bond lengths in O_2 and O_2^- at the HF/6-31G* level, respectively. The $^3B_2(^3\Sigma_u^-)$ curve was calculated for r(Mg–X) less than 1.0 Å by optimizing r(O–O) at each value of r(Mg–X). This yields the minimum energy path as a function of r(Mg–X) on the $^3B_2$ surface. The surfaces for r(Mg–X) between 1.0 and 1.6 Å could not be determined due to a lack of convergence of the single configuration wave functions. The two ionic curves ($^3B_2$ and $^3A_2$) were then scaled in energy relative to the $^3B_1$ curve by subtracting 79.5 kJ mol^{-1}, in order to give the correct dissociation energies to Mg + O_2 that were calculated from eq 9 (Table III). Now consider attack of a Mg atom along the C_{2v} axis. At long range, reaction 1 proceeds along the covalent $^3B_1$ surface. A nonadiabatic transition onto the $^3A_2$ surface may then occur by a charge transfer between the Mg and O_2, with perhaps a further transition onto the $^3B_2$ surface. The important result is that there is a significant electronic barrier at the crossing point between the $^3B_1$ and $^3A_2$ surfaces, equal to 52 kJ mol^{-1} at the intersection of the curves shown in Figure 6. This arises because the charge transfer occurs at r(Mg–X) = 2.6 Å, so the covalent $^3B_1$ surface has already begun to demonstrate short-range electronic repulsion between the reactants. Thus, this reaction proceeds by a charge transfer that is quite unlike the classical long-range "harpoon mechanism".[6]

The presence of the barrier was checked by recalculating the relevant parts of the potential energy curves with a correction for electron correlation by means of fourth-order Moller–Plesset theory.[27] The barrier still occurred at the same value of r(Mg–X), with the barrier height reduced to 29 kJ mol^{-1}. We also established that a barrier was present for other geometries of attack. For example, at the HF/6-31G* level, the barrier for end-on attack by Mg on O_2 is 48 kJ mol^{-1} at r(Mg–X) = 2.9 Å; when attack occurs at an Mg–X–O angle of 45°, the barrier height drops to 35 kJ mol^{-1} at r(Mg–X) = 2.7 Å.

We now describe an extrapolation of $k_1(T)$ from the measured temperature range 350–624 K to temperature regimes characteristic of the mesosphere and of combustion processes. For this purpose, we employed the Troe formalism,[19] which is based on a simplified form of RRKM theory. The calculation proceeds by determining the strong collision rate constant for the reverse unimolecular decomposition reaction in the low-pressure limit, k_0^{sc}. The rate constant for the strong collision recombination reaction is then derived by detailed balancing through the equilibrium constant:[19]

$$k_{rec,0}^{sc} = K_{eq}k_0^{sc} \tag{10}$$

$k_{rec,0}$ is then expressed as a product of the strong collision rate constant $k_{rec,0}^{sc}$ and the weak collision efficiency, β_c, for the energy transfer:

$$k_{rec,0} = \beta_c k_{rec,0}^{sc} \tag{11}$$

where β_c lies between 0 and 1 and is obtained by comparing $k_{rec,0}^{sc}$ with experiment. The temperature dependence of β_c is given by

$$\beta_c/(1-\beta_c^{1/2}) = -\langle\Delta E\rangle/(F_E RT) \tag{12}$$

where $\langle\Delta E\rangle$ is the average energy transferred per collision. This quantity is usually determined through eq 12 if β_c is known at a particular temperature. In the case of N_2 and He as third bodies, $\langle\Delta E\rangle$ has generally been found to be proportional to T^n where $-0.5 < n < 0.5$.[28] The strong collision rate constant for the unimolecular dissociation reaction may be expressed as[19]

$$k_0^{sc} = [Z_{LJ}\rho(E_0)RT\exp(-E_0/RT)F_E F_{anh}F_{rot}F_{corr}]/Q_{vib} \tag{13}$$

where Z_{LJ} is the Lennard-Jones reference collision frequency between MgO_2 and M, calculated in terms of the appropriate collision diameter and reduced collision integral; $\rho(E_0)$ is the density of states of MgO_2 at the critical energy, E_0; and F_E, F_{anh}, and F_{rot} are correction terms arising from the energy dependence of the density of states, from the vibrational anharmonicity of MgO_2, and from rotational contribution to the density of states, respectively. F_{corr} is a correction factor that accounts for the coupling between different degrees of freedom and is usually taken as unity. Q_{vib} is the vibrational partition function. Finally, in order to apply this formalism to reaction 1, which has a barrier of height E_b (including zero-point energies) in the entrance channel, we employ the relationship

$$E_0 = D_0(Mg–O_2) + E_b \tag{14}$$

The recent work of Bauschlicher *et al.*[5] has shown that the $^3\Sigma_g^-$ state of MgO_2 is the most stable.[5] However, as indicated in Figure 9, there is a barrier to insertion of the Mg into the O–O bond. We cannot tell from the level of *ab initio* theory employed in the present study whether the barrier between the superoxide $MgO_2(^3A_2)$ and linear O–Mg–O is higher than the initial barrier between the covalent ($^3B_1$) and ionic ($^3A_2$) reactants and thus whether linear $MgO_2(^3\Sigma_g^-)$ can in fact be formed in reaction 1. Therefore, we applied the Troe formalism[19] assuming that either $MgO_2(^3A_2)$ or $MgO_2(^3\Sigma_g^-)$ is the exclusive product. The molecular parameters for both states of MgO_2 were taken from Bauschlicher *et al.*[5] However, a satisfactory fit to the experimental data with sensible values for the adjustable parameters (see below) could only be obtained with $MgO_2(^3\Sigma_g^-)$ as the recombination product.

The data used in the calculations are listed in Table IV. The choice of the Lennard-Jones parameters σ(MgO–M) and

TABLE V: Comparison of *ab Initio* Geometries and Bond Energies for CaO_2

	state	r_{Ca-O}/Å	r_{O-O}/Å	$D_e(Ca-O_2)$/ (kJ mol^{-1})
	O–Ca–O, C_{2v} Symmetry			
this study (HF/GEN)[a]	$^3A_2$	2.21	1.28	171
Bauschlicher *et al.*[5]	$^3A_2$	2.20	1.34	184
	Liner O–Ca–O			
Bauschlicher *et al.*[5]	$^3\Sigma_g^-$	2.15	–	166
	Linear Ca–O–O			
this study (HF/GEN)[a]	*b*	2.03	1.29	122

[a] See text. [b] Electronic symmetry not determined.

$\epsilon(MgO_2–M)/k$ has to be assumed in order to calculate the Lennard-Jones collision frequency between MgO_2 and M. This choice was based on our previous work.[9b,9c] It should be noted that the resulting values of Z_{LJ} are larger than typical gas kinetic collision frequencies, in accord with a recent analysis by Lenvay and Schatz.[29] The other adjustable parameters are the barrier height, E_b, and the T-dependence of $\langle\Delta E\rangle$, n. The results of applying the Troe formalism[19] to reaction 1 are listed in Table IV for M = N_2 and He at 350 K. The collision efficiencies $\beta_c(N_2) = 0.70$ and $\beta_c(He) = 0.25$ were obtained by comparing the calculated strong collision rate coefficients, $k_{rec,0}^{sc}$, with the experimental data from this study for N_2 (*i.e.*, eq 7) and from Vinckier *et al.*[2] for He, at 350 K. Although these collision efficiencies are about twice the efficiencies considered typical for these third bodies, they are still in accord with a wide body of data.[19] Highly satisfactory fits to $k_1(T)$ over the experimental temperature ranges were then obtained with a barrier of 26 kJ mol^{-1} and very small T-dependences of $\langle\Delta E\rangle$ (see Table IV). These fits are illustrated in Figure 4. The barrier height is roughly in accord with the height derived from the *ab initio* calculations described earlier.

It is necessary at this point to establish that the experimental measurements of $k_1(T)$ are close to the rate coefficient at the low-pressure limit, $k_{rec,0}$. We therefore followed our previous procedure,[9b,9c] based on the work of Luther and Troe.[30] The calculation requires an estimate of the high-pressure rate constant, $k_{rec,0}$. In this case, we set

$$k_{rec,0} = Z(T)\exp(-E_b/RT) \qquad (15)$$

where the preexponential collision frequency is calculated in terms of the orbiting criteria on the attractive surface due to the long-range dispersion force between Mg and O_2.[9b] The dispersion coefficient, $C_6 = 1.13 \times 10^7$ J mol^{-1} Å^6, was calculated from the London formula[31] with the polarizabilities of Mg and O_2 taken from ref 32. This yielded $Z(T) = 6.04 \times 10^{-10}(T/300\text{ K})^{1/6}$ cm^3 molecule^{-1} s^{-1}. The calculation[9b,9c,30] of $k_1/k_{rec,0}$ indicates that in the present experiments this quantity ranged from 0.84 (350 K, 30.0 Torr of N_2) to 0.94 (624 K, 12.7 Torr). Thus, our experiments are essentially in the low-pressure limit.

$k_1(T)$ can now be extrapolated outside the experimental temperature range of the present study and that of Vinckier *et al.*[2] This is illustrated in Figure 4 from 200 to 2000 K. The recommended fits over the temperature range 120–2000 K are given by

$$\log_{10}(k_1(Mg+O_2+N_2)/\text{cm}^6\text{ molecule}^{-2}\text{ s}^{-1}) = -392.7 + 439.1x - 203.2x^2 + 42.56x^3 - 3.413x^4$$

$$\log_{10}(k_1(Mg+O_2+He)/\text{cm}^6\text{ molecule}^{-2}\text{ s}^{-1}) = -394.5 + 442.4x - 205.0x^2 + 42.94x^3 - 3.436x^4$$

where $x = \log_{10}(T)$. Since the fitted parameters of this polynomial are not physically meaningful, we have not assigned individual uncertainties to them. Instead, we have estimated that the uncertainty in k_1 is ±30%, obtained by comparison with the calculated fit to the experimental data.

Finally, we described in the Introduction the shock-tube study by Hodgson and Mackie[12] of the reaction between Mg and O_2 at high temperatures. Those authors considered that a recombination reaction was unlikely because they were unaware that MgO_2 had been shown to exist.[3,4] However, as we argued above, reaction 3 is most likely to be too endothermic to have the bimolecular rate coefficient they determined. If, in fact, they were observing loss of atomic Mg due to reaction 1, at an Ar carrier gas pressure of about 164 Torr, then their measurement of k_3 would translate into $k_1(2000\text{K}) = (1.0 \pm 0.6) \times 10^{-31}$ cm^6 molecule^{-2} s^{-1}. Inspection of Figure 4 indicates that this result is in good accord with our extrapolated values. Unfortunately, $D_0(Mg–O_2)$ is so small (Table III) that the equilibrium concentration of MgO_2 at 2000 K in the shock tube would be negligible. Thus, either the nascent MgO_2 is removed by further reaction in the shock tube or $D_0(Mg–O)$ and $D_0(Mg–O_2)$ are much greater than indicated by *ab initio* calculations.[5,14] We have noted elsewhere[1] the apparent discrepancy between the bond energies of metal superoxides obtained from theory and those that are required to explain the kinetics of recombination reactions.

Ca + O_2 + M. Reaction 2 does not appear to have been studied previously in the gas phase, although the reaction has been observed to occur when Ca and O_2 are co-deposited into an inert gas matrix.[3] The positive temperature dependences of k_2(M=N_2,He) at low temperatures (Figure 8) indicate that this reaction is probably also governed by a barrier, although it must be much smaller than that in the case of reaction 1. Reaction 2 may also be compared with the reaction K + O_2 + M, which has a conventional negative T-dependence.[9c] $k_2(T)$ is smaller by about a factor of 10 at 250 K for the corresponding third bodies.

We now present a theoretical treatment for reaction 2 that is similar to that given above for reaction 1. Theoretical calculations on the different forms of CaO_2 are listed in Table V. Our calculations were carried out with an extended basis set for Ca recommended by Langhoff *et al.*[14] and a basis set for O that we have employed previously.[9c] For $CaO_2(^3A_2)$, we are in good agreement with the geometry and bond energy determined by Bauschlicher *et al.*[5] and concur that this is the lowest triplet state. The Troe formalism[19] was then applied to reaction 2, which was assumed to form $CaO_2(^3A_2)$ exclusively. The molecular parameters for CaO_2 were taken from ref 5. As before, E_b, n, and the Lennard-Jones parameters were the only adjustable parameters. The results of applying the Troe formalism[19] to reaction 2 are listed in Table VI for M = N_2 and He at 300 K. Satisfactory fits to $k_2(T)$ over the experimental temperature ranges were obtained with a barrier of 5.5 kJ mol^{-1} and with $\langle\Delta E\rangle$ independent of temperature. The fits to the experimental data are illustrated in Figure 8.

The high-pressure rate constant for reaction 2, $k_{rec,\infty}$, can be estimated in the same way as for reaction 1 (eq 15). The dispersion coefficient between Ca and O is then $C_6 = 2.31 \times 10^7$ J mol^{-1} Å^6, and $Z(T) = 6.74 \times 10^{-10}(T/300\text{ K})^{1/6}$ cm^3 molecule^{-1} s^{-1}. In the present data set, $k_2(T)/k_{rec,0}$ varies from 0.73 (335 K, 94.4 Torr of N_2) to 0.97 (1106 K, 19.2 Torr of N_2), so the data are reasonably close to the data of the low-pressure limit. However, this calculation does suggest that at temperatures below 300 K it should be possible to observe significant falloff to second-order behavior at pressures below 1 atm, although this would be difficult to measure in our experimental system because of the problems with the Ca atom precursors described above. $k_1(T)$ can now be extrapolated outside the experimental temperature range of the present study. This is illustrated in Figure 4 from 120 to 2000

TABLE VI: Extrapolation of Rate Data for the Reaction Ca + O_2 + M[a]

Input Parameters for the $CaO_2(^3A_2)$ Molecule

r_{Ca-O} = 2.20 Å, r_{O-O} = 1.34 Å, I_{ABC} = 1.15 × 10^5 amu^3 Å^6, ν_1 = 419 cm^{-1}, ν_2 = 368 cm^{-1}, ν_3 = 1101 cm^{-1}, $D_0(Ca-O_2)$ = 184 kJ mol^{-1}, E_b = 5.5 kJ mol^{-1}, E_0 = 189.5 kJ mol^{-1}

Data for Ca + O_2 + N_2 at 300 K

$\sigma(CaO_2-N_2)$ = 5.0 Å, $\epsilon(CaO_2-N_2)/k$ = 500 K, Z_{LJ} = 8.65 × 10^{-10} cm^3 molecule^{-1} s^{-1}, s = 3, m = 2, r = 0, Q_{vib} = 1.40, a = 0.990, $\rho(E_0)$ = 0.069, F_E = 1.025, F_{anh} = 1.72, F_{rot} = 36.3, F_{corr} = 1, K_{eq} = 3.79 × 10^8 cm^3 molecule^{-1}, k_0^{sc} = 6.91 × 10^{-39} cm^3 molecule^{-1} s^{-1}, $k_{rec,0}^{sc}$ = 2.62 × 10^{-30} cm^6 molecule^{-2} s^{-1}, β_c = 0.73, $\langle\Delta E\rangle$ = −12.8$(T/300)^{0.0}$ kJ mol^{-1}

Data for Ca + O_2 + He at 300 K

$\sigma(CaO_2-He)$ = 4.0 Å, $\epsilon(CaO_2-He)/k$ = 400 K, Z_{LJ} = 9.57 × 10^{-10} cm^3 molecule^{-1} s^{-1}, k_0^{sc} = 9.21 × 10^{-39} cm^3 molecule^{-1} s^{-1}, $k_{rec,0}^{sc}$ = 3.49 × 10^{-30} cm^6 molecule^{-2} s^{-1}, β_c = 0.27, $\langle\Delta E\rangle$ = −1.43$(T/300)^{0.0}$ kJ mol^{-1}

[a] For the definition of symbols not in the present text, see ref 19.

K. The recommended fits over this temperature range are given by

$$\log_{10}(k(Ca+O_2+N_2)/cm^6\ molecule^{-2}\ s^{-1}) = -97.75 + 84.66x - 39.85x^2 + 8.522x^3 - 0.7093x^4$$

$$\log_{10}(k(Ca+O_2+He)/cm^6\ molecule^{-2}\ s^{-1}) = -93.67 + 78.02x - 35.76x^2 + 6.369x^3 - 0.5899x^4$$

where $x = \log_{10}(T)$ and the estimated uncertainty in k_2 is ±30%, obtained by comparison with the experimental data.

Implications for the Chemistry of Mg and Ca in the Mesosphere. Reaction 1 is so slow at a temperature of 200 K, which is typical of the atmosphere at 90 km,[10] that the lifetime of a Mg atom with respect to recombination with O_2 is about 4 years. The only other likely source of oxidation of atomic Mg is the reaction

$$Mg + O_3 \rightarrow MgO + O_2 \qquad (16)$$

This reaction has been observed to proceed in an inert gas matrix.[4] However, if reaction 16 is slow, or if MgO is rapidly reduced back to atomic Mg by reaction with atomic O, then a large fraction of the Mg which ablates from meteoroids is probably in the atomic form in the upper atmosphere.

Reaction 2 is sufficiently fast to compete with the reaction

$$Ca + O_3 \rightarrow CaO + O_2 \qquad (17)$$

at mesospheric temperatures.[33] Hence, it probably plays an important role in the atmospheric chemistry of Ca, as NaO_2 does for Na chemistry.[10] It is particularly interesting to note that reaction 2 and the reaction

$$Na + O_2 + N_2 \rightarrow NaO_2 + N_2 \qquad (18)$$

have opposing temperature dependences at low temperatures, since $k_{18}(T) = 4.7 \times 10^{-30}(T/200\ K)^{-1.22}$ cm^6 molecule^{-2} s^{-1}.[1,9b,10] At mid-latitudes, the upper mesosphere *cools* to about 170 K in summer from a winter maximum of about 220 K. The ratio k_{18}/k_2 thus changes from about 3.4 in winter to 9.0 in summer. This predicts that relatively more Na will be converted to NaO_2, than Ca to CaO_2, in summer. All other factors remaining constant, the ratio of atomic Na to Ca should then decrease by a factor of about 3 between winter and summer, as has indeed been observed.[11]

Acknowledgment. This work was supported under Grant ATM-8820225 from the National Science Foundation, Grant ATM-900003P from the Pittsburgh Supercomputing Center, and Grant GR/G 45021 from the Science and Engineering Research Council.

References and Notes

(1) Plane, J. M. C. In *Gas-Phase Metal Reactions*; Fontijn, A., Ed.; Elsevier: Amsterdam, 1992.
(2) Vinckier, C.; Christiaens, P.; Hendrickx, M. In *Gas-Phase Metal Reactions*; Fontijn, A., Ed.; Elsevier: Amsterdam, 1992.
(3) Ault, B. S.; Andrews, L. *J. Chem. Phys.* **1975**, *62*, 2312.
(4) Andrews, L.; Prochaska, E. S.; Ault, B. S. *J. Chem. Phys.* **1978**, *69*, 556.
(5) Bauschlicher, C. W.; Partridge, H.; Sodupe, M.; Langhoff, S. R. *J. Phys. Chem.* **1992**, *96*, 9259.
(6) Grice, R.; Herschbach, D. R. *Mol. Phys.* **1974**, *27*, 159.
(7) Husain, D.; Plane, J. M. C.; Chen, C. X. *J. Chem. Soc., Faraday Trans. 2* **1985**, *81*, 1465, 1619; **1985**, *81*, 561, 769.
(8) Husain, D.; Plane, J. M. C.; Chen, C. X. *J. Chem. Soc., Faraday Trans. 2* **1985**, *81*, 1675. Plane, J. M. C.; Husain, D. *J. Phys. Chem.* **1986**, *90*, 501. Plane, J. M. C.; Husain, D. *J. Chem. Soc., Faraday Trans. 2* **1986**, *82*, 897.
(9) (a) Husain, D.; Marshall, P.; Plane, J. M. C. *J. Chem. Soc., Faraday Trans. 2* **1985**, *81*, 301. (b) Plane, J. M. C.; Rajasekhar, B. *J. Phys. Chem.* **1988**, *92*, 3884; **1989**, *93*, 3135. (c) Plane, J. M. C.; Rajasekhar, B.; Bartolotti, L. *Ibid.* **1990**, *94*, 4161.
(10) Plane, J. M. C. *Int. Rev. Phys. Chem.* **1991**, *10*, 55.
(11) Granier, C.; Jegou, J. P.; Megie, G. *Geophys. Res. Lett.* **1985**, *12*, 655.
(12) Hodgson, A.; Mackie, J. C. *Combust. Flame* **1979**, *35*, 323.
(13) Kashireninov, O. E.; Manelis, G. B.; Repka, L. F. *Zh. Fiz. Khim.* **1982**, *56*, 1030; *Russ. J. Phys. Chem.* **1982**, *56*, 630.
(14) Langhoff, S. R.; Bauschlicher, C. W.; Partridge, H. *J. Chem. Phys.* **1986**, *84*, 4474.
(15) JANAF Thermochemical Tables, 3rd ed.; Chase, M. W., Jr., Davies, C. A., Downey, J. R., Jr., Frurip, D. J., McDonald, R. A., Syverud, A. N., Eds.; *J. Phys. Chem. Ref. Data* **1985**, *14*.
(16) Irvin, J. A.; Dagdigian, P. J. *J. Chem. Phys.* **1980**, *73*, 176.
(17) Plane, J. M. C.; Nien, C-F.; Rajasekhar, B. *J. Phys. Chem.* **1992**, *96*, 1296.
(18) Plane, J. M. C.; Nien, C.-F. *J. Phys. Chem.* **1990**, *94*, 5255.
(19) Troe, J. *J. Chem. Phys.* **1977**, *66*, 4745, 4758; *J. Phys. Chem.* **1979**, *83*, 114.
(20) Mitchell, A. C. G.; Zemansky, M. W. *Resonance Radiation and Excited Atoms*; Cambridge University Press: London, 1934.
(21) Silver, J. A. *J. Chem. Phys.* **1984**, *81*, 5125.
(22) Ager, J. W., III.; Howard, C. J. *J. Chem. Phys.* **1986**, *85*, 3469.
(23) Plane, J. M. C. *J. Phys. Chem.* **1987**, *91*, 6552.
(24) Edelstein, S. A.; Davidovits, P. *J. Chem. Phys.* **1971**, *55*, 5164.
(25) Frisch, M. J.; Binkley, J. S.; Schlegel, H. B.; Ragavachari, K.; Melius, C. F.; Martin, R. L.; Stewart, J. J. P.; Bobrowich, F. W.; Rohlfing, C. M.; Kahn, L. R.; Defrees, D. J.; Seeger, R.; Whiteside, R. A.; Fox, D. J.; Fleuder, E. M.; Pople, J. A. *Gaussian 86*; Carnegie-Mellon Quantum Chemistry Publishing Unit: Pittsburgh, PA, 1984.
(26) Plane, J. M. C.; Rajasekhar, B.; Bartolotti, L. *J. Phys. Chem.* **1989**, *93*, 3141.
(27) Moller, C.; Plesset, M. S. *Phys. Rev.* **1934**, *46*, 618.
(28) Heymann, M.; Hippler, H.; Plach, H. J.; Troe, J. *J. Chem. Phys.* **1987**, *87*, 3867.
(29) Lenvay, G.; Schatz, G. C. *J. Phys. Chem.* **1992**, *96*, 3753.
(30) Luther, K.; Troe, J. *Proceedings of the 17th Symposium (International) on Combustion*; The Combustion Institute: Pittsburgh, PA, 1978; p 535.
(31) Maitland, G. C.; Rigby, M.; Brian Smith, E.; Wakeham, W. A. *Intermolecular Forces, Their Origin and Determination*; Clarendon Press: Oxford, 1987.
(32) *Handbook of Physics and Chemistry*, 70th ed.; Weast, R. C., Ed.; CRC Press: Boca Raton, FL, 1990.
(33) Helmer, M.; Allen, M. R.; Plane, J. M. C. *J. Chem. Soc., Faraday Trans.* **1993**, *89*, 763.